Thin-Walled Structures 127 (2018) 688–699

Contents lists available at ScienceDirect

Thin-Walled Structures

journal homepage: www.elsevier.com/locate/tws

Full length article

Buckling of a standing corrugated sandwich plate subjected to body force and terminal load

Fei-Hao Li[a,b], Bin Han[a,c,d,*], Qian-Cheng Zhang[a,b], Feng Jin[a,b], Tian Jian Lu[a,b,*]

[a] MOE Key Laboratory for Multifunctional Materials and Structures, Xi'an Jiaotong University, Xi'an 710049, PR China
[b] State Key Laboratory for Strength and Vibration of Mechanical Structures, Xi'an Jiaotong University, Xi'an 710049, PR China
[c] School of Mechanical Engineering, Xi'an Jiaotong University, Xi'an 710049, PR China
[d] School of Engineering, Brown University, Providence, RI 02912, USA

ARTICLE INFO

Keywords:
Corrugated sandwich
Stability analysis
Zig-zag
Body force
Shear effect

ABSTRACT

The global buckling behavior of a vertically standing corrugated sandwich plate subjected to body force and terminal load is analyzed through an improved first order zig-zag shear deformation theory, with the transverse shear effect of face sheets taken into account. When the face sheets are relatively thick and/or the sandwich plate has relatively large thickness to height ratios, the transverse shear effect of the face sheets affects significantly the critical buckling load. The effect becomes more obvious when body force rather than terminal load is applied on the clamped plates. The influence of geometric parameters on critical buckling parameters is also explored.

1. Introduction

Sandwich plates with periodic lattice cores, either two- or three-dimensional, possess superior bending stiffness, strength and shock resistance with respect to monolithic plate of the same mass. They also present opportunities for additional functionalities, such as energy absorption, active cooling and vibration/noise control. In particular, due to simple fluid-through topology and relatively easy fabrication, corrugated sandwich plates have enjoyed widespread applications in areas of packaging, building construction and high-speed railway transportation [1,2]. Recently, it has been envisioned that corrugated sandwich plates are attractive candidate for constructing oversized lightweight structures with multi-functionalities, such as large-scale gates and towering walls. In practice, when such a large structure exhibits accelerated movement, its self-weight or acceleration-induced body force as a kind of in-plane distributed load can play an important role in affecting its stability and natural frequencies. Considering the effect of body forces is therefore necessary in the stability analysis and design of a standing plate especially when it has relatively large scale.

Existing theoretical studies on the buckling and vibration behaviors of standing monolithic or laminated plates subjected to body forces are mainly carried out with the classical plate theory or the Mindlin plate theory. Considering the effect of body forces, Sussaman and Wang [3] studied the elastic stability of a simply-supported thin rectangular plate under linearly variable compressive stresses. Brown [4] investigated the elastic buckling behavior of plates with a variety of boundary conditions under three different distributions of in-plane loading. Using the Levy and Ritz method, Wang et al. [5,6] solved the gravity-induced buckling problem of a standing vertical plate under several boundary conditions.

Apart from body forces, the influence of top (terminal) load and plate aspect ratio (e.g., ratio of width to height) on the buckling performance of standing plates have been explored. For instance, based on the Mindlin plate theory, Bodaghi and Saidi [7] presented an exact analytical solution for the stability of a vertical moderately thick laminated plate subjected to self-weight and top load.

In addition to buckling, Fauconneau and Marangoni [8], Yu and Wang [9,10] demonstrated that self-weight affects considerably the natural frequency and mode shape of a standing heavy plate.

Existing theories for modeling the displacement fields and characterizing the buckling/vibration behaviors of laminated composite plates and sandwich plates include: the classical theory, the higher-order equivalent single layer theory, the zig-zag theory, the layerwise theory, and the mixed theories [11,12]. These theories differ mainly in the shape functions of shear deformation and the modeling of inter-laminar continuity stresses. Up to now, the global buckling analysis of standing corrugated sandwich plates subjected to in-plane distributed load is yet studied. Further, most existing theories assume that the face sheets of sandwich plates are thin and hard so that their shear effect can be ignored [13,14]. Recently, Krzysztof et al. [15] developed a seven-layer sandwich beam model and found that the shear deformation of face sheets should be taken into account when the sandwich core is

* Corresponding authors at: MOE Key Laboratory for Multifunctional Materials and Structures, Xi'an Jiaotong University, Xi'an 710049, PR China.
E-mail addresses: hanbinghost@mail.xjtu.edu.cn (B. Han), tjlu@mail.xjtu.edu.cn (T.J. Lu).

https://doi.org/10.1016/j.tws.2018.03.013
Received 24 May 2017; Received in revised form 7 February 2018; Accepted 11 March 2018
Available online 23 March 2018
0263-8231/

relatively soft.

The buckling behavior of a vertical corrugated sandwich plate under body force and/or terminal load remains to be explored. Relative to a monolithic or laminated plate of equal mass, the corrugated sandwich plate may be more stable because of its in-plane orthotropic mechanical property and excellent flexural rigidity, especially when the main bending direction is coincident with the in-plane loading direction. This study aims to address the issue by employing the first order shear deformation theory and the improved zig-zag formulation [16] to describe the kinematics of the corrugated sandwich plate subjected to different combinations of boundary constraints (e.g., free, simply supported and clamped). During the analysis, the corrugated core is modelled as an equivalent orthotropic layer. Different from previous studies on similar problems, the proposed displacement field takes the shear effect of face sheets into account. The principle of minimum total potential energy and the p-Ritz method are employed to solve the global buckling problem. The theoretical predictions are validated by comparing with existing results when the sandwich plate is degenerated to a monolithic plate as well as finite element simulation results when the corrugated sandwich plates are of concern. The influence of face sheet shear effect on critical buckling loads is quantified for face sheets made of metal, functional graded material (FGM) and carbon fiber-reinforced composite (T700/3234). The effects of face sheet thickness, core relative density, corrugation inclination angle, and sandwich plate aspect ratio are also explored.

2. Formulation

2.1. Problem definition

With reference to Fig. 1a, consider the global buckling behavior of a vertically standing corrugated sandwich plate of width W and height L subjected to both gravitational force and terminal load. Let $a = W/L$ define the aspect ratio of the sandwich plate, and let the Cartesian coordinate system be located at the geometrical center of the plate. Fig. 1b depicts the geometric parameters of the sandwich cross-section: total thickness h, core height c, face sheet thickness t_f, core plate thickness t_c, and corrugation inclination θ. The terminal load P is applied at the center line of the top cross-section, while the gravity G is exerted on the whole sandwich structure.

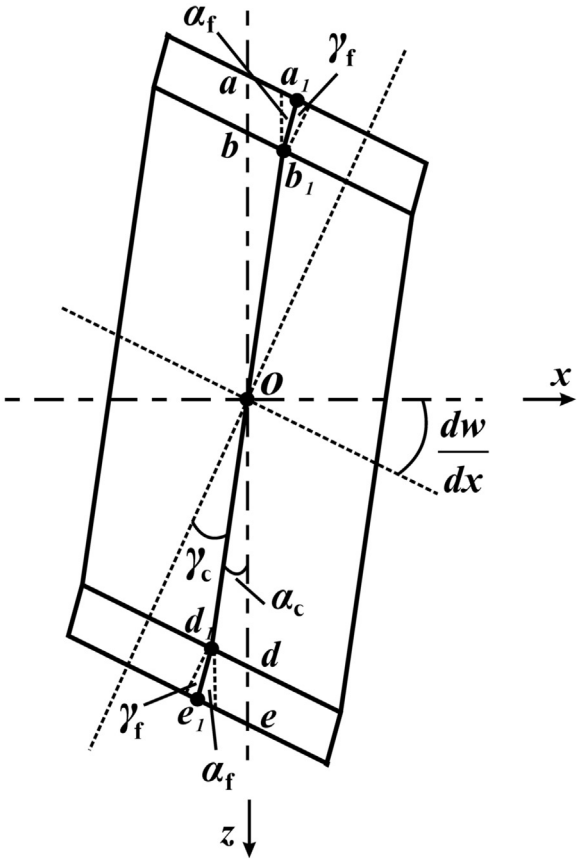

Fig. 2. Displacement hypothesis of improved zig-zag form (x-z plane).

2.2. Kinematics

The present study treats the discrete corrugated core of Fig. 1b as an equivalent uniform orthogonal layer. Then, based on the first order shear deformation theory and the improved zig-zag formulation [16], Fig. 2 presents the displacement hypothesis for the sandwich with equivalent core. Upon deformation, the straight line *abode* originally perpendicular to the mid-surface moves to a new position $a_1b_1od_1e_1$. Let α_c and α_f represent the rotation angle of the core and the face sheets in

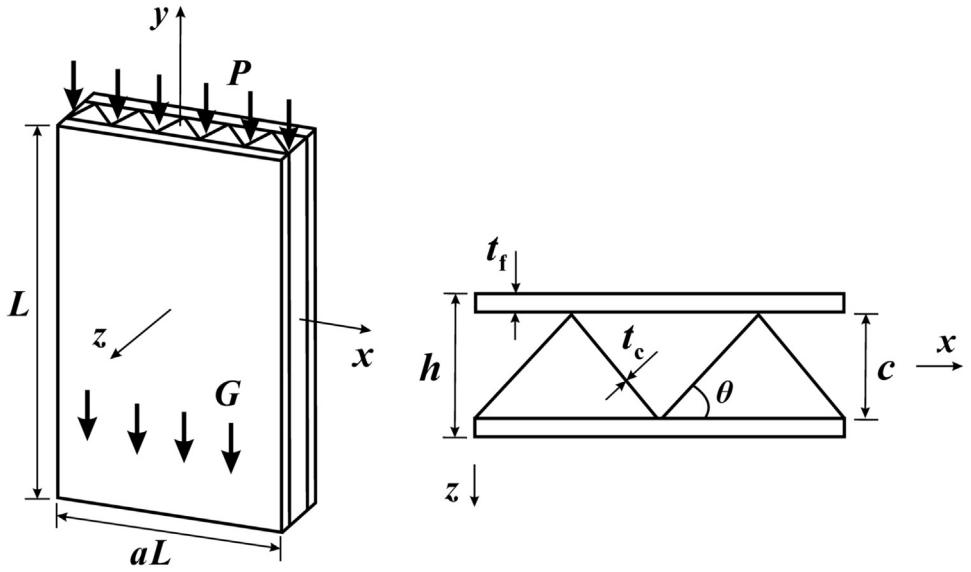

Fig. 1. (a) A vertically standing corrugated sandwich plate under combined body force and terminal load; (b) cross-sectional view of corrugated sandwich.

x-z plane, and let γ_c and γ_f denote the shear angle of the core and the face sheets, respectively. Relevant assumptions made by the hypothesis are:

(1) First order shear deformation is assumed when shear deformation of both the core and the face sheets is considered;
(2) The core and the face sheets are assumed to have the same transverse displacement $w(x, y)$, but their rotations may be different;
(3) Buckling analysis is limited to linear-elastic range;
(4) No relative slippage occurs at the interface between the core and the face sheets;
(5) The two face sheets have the same thickness and are made of the same material, and hence possess the same rotation.

In view of the forgoing hypothesis, the in-plane displacement field of the sandwich can be written as:

- Top face sheet ($-h/2 \le z \le -c/2$):

$$\begin{aligned} u^{t}(x, y, z) &= \frac{c}{2}\alpha_c(x, y) - (z + \frac{c}{2})\alpha_f(x, y) \\ v^{t}(x, y, z) &= \frac{c}{2}\beta_c(x, y) - (z + \frac{c}{2})\beta_f(x, y) \end{aligned} \tag{1}$$

- Corrugated core ($-c/2 < z < c/2$):

$$\begin{aligned} u^{c}(x, y, z) &= -z\alpha_c(x, y) \\ v^{c}(x, y, z) &= -z\beta_c(x, y) \end{aligned} \tag{2}$$

- Bottom face sheet ($c/2 \le z \le h/2$):

$$\begin{aligned} u^{b}(x, y, z) &= -\frac{c}{2}\alpha_c(x, y) - (z - \frac{c}{2})\alpha_f(x, y) \\ v^{b}(x, y, z) &= -\frac{c}{2}\beta_c(x, y) - (z - \frac{c}{2})\beta_f(x, y) \end{aligned} \tag{3}$$

where β_c and β_f represent separately the rotation angle of the core and the face sheets in y-z plane.Correspondingly, the strains associated with the displacement field are:

- Top/bottom face sheet:

$$\{\varepsilon\}^{f} = \begin{bmatrix} \varepsilon_x^{t,b} \\ \varepsilon_y^{t,b} \\ \gamma_{xy}^{t,b} \\ \gamma_{yz}^{t,b} \\ \gamma_{xz}^{t,b} \end{bmatrix} = \begin{bmatrix} u^{t,b}{}_{,x} \\ v^{t,b}{}_{,y} \\ u^{t,b}{}_{,y} + v^{t,b}{}_{,x} \\ v^{t,b}{}_{,z} + w_{,y} \\ u^{t,b}{}_{,z} + w_{,x} \end{bmatrix} = \begin{bmatrix} \pm\frac{c}{2}\frac{\partial\alpha_c}{\partial x} - (z \pm \frac{c}{2})\frac{\partial\alpha_f}{\partial x} \\ \pm\frac{c}{2}\frac{\partial\beta_c}{\partial y} - (z \pm \frac{c}{2})\frac{\partial\beta_f}{\partial y} \\ \pm\frac{c}{2}(\frac{\partial\alpha_c}{\partial y} + \frac{\partial\beta_c}{\partial x}) - (z \pm \frac{c}{2})(\frac{\partial\alpha_f}{\partial y} + \frac{\partial\beta_f}{\partial x}) \\ -\beta_f + \frac{\partial w}{\partial y} \\ -\alpha_f + \frac{\partial w}{\partial x} \end{bmatrix} \tag{4}$$

- Corrugated core:

$$\{\varepsilon\}^{c} = \begin{bmatrix} \varepsilon_x^{c} \\ \varepsilon_y^{c} \\ \gamma_{xy}^{c} \\ \gamma_{yz}^{c} \\ \gamma_{xz}^{c} \end{bmatrix} = \begin{bmatrix} u^{c}{}_{,x} \\ v^{c}{}_{,y} \\ u^{c}{}_{,y} + v^{c}{}_{,x} \\ v^{c}{}_{,z} + w_{,y} \\ u^{c}{}_{,z} + w_{,x} \end{bmatrix} = \begin{bmatrix} -z\frac{\partial\alpha_c}{\partial x} \\ -z\frac{\partial\beta_c}{\partial y} \\ -z(\frac{\partial\alpha_c}{\partial y} + \frac{\partial\beta_c}{\partial x}) \\ -\beta_c + \frac{\partial w}{\partial y} \\ -\alpha_c + \frac{\partial w}{\partial x} \end{bmatrix} \tag{5}$$

where $\{\varepsilon\}^{f}$ and $\{\varepsilon\}^{c}$ are the strain vectors of the face sheets and the (equivalent) corrugated core, respectively.

2.3. Constitutive equations

To verify the effectiveness of the displacement hypothesis detailed in the previous section, face sheets made of three different materials are considered: metal, FGM and fiber-reinforced composite. The stress-strain relationship of the face sheets and the equivalent core can be concisely expressed as:

$$\{\sigma\}^{f,c} = [\mathbf{C}]^{f,H}\{\varepsilon\}^{f,c} \tag{6}$$

where $\{\sigma\}^{f}$ and $\{\sigma\}^{c}$ represent the stress vectors of the face sheets and the equivalent core, $[\mathbf{C}]^{f}$ is the stiffness matrix of the face sheets, and $[\mathbf{C}]^{H}$ is the equivalent stiffness matrix of the core. When written explicitly, they are:

$$\{\boldsymbol{\sigma}\}^{f} = [\sigma_x \quad \sigma_y \quad \tau_{xy} \quad \tau_{yz} \quad \tau_{xz}]^{f\,T} \tag{7}$$

$$\{\boldsymbol{\varepsilon}\}^{f} = [\varepsilon_x \quad \varepsilon_y \quad \varepsilon_{xy} \quad \varepsilon_{yz} \quad \varepsilon_{xz}]^{fT} \tag{8}$$

$$[\mathbf{C}]^{f} = \begin{bmatrix} \frac{E_1^f}{1-\nu_{12}^f\nu_{21}^f} & \frac{\nu_{21}^f E_1^f}{1-\nu_{12}^f\nu_{21}^f} & 0 & 0 & 0 \\ \frac{\nu_{12}^f E_2^f}{1-\nu_{12}^f\nu_{21}^f} & \frac{E_2^f}{1-\nu_{12}^f\nu_{21}^f} & 0 & 0 & 0 \\ 0 & 0 & G_{12}^f & 0 & 0 \\ 0 & 0 & 0 & G_{23}^f & 0 \\ 0 & 0 & 0 & 0 & G_{13}^f \end{bmatrix} \tag{9}$$

$$[\mathbf{C}]^{H} = \begin{bmatrix} C_{11}^H & C_{12}^H & 0 & 0 & 0 \\ C_{12}^H & C_{22}^H & 0 & 0 & 0 \\ 0 & 0 & C_{44}^H & 0 & 0 \\ 0 & 0 & 0 & C_{55}^H & 0 \\ 0 & 0 & 0 & 0 & C_{66}^H \end{bmatrix} \tag{10}$$

in which the expressions of C_{ij}^{H} are referred to Han et al. [1]. Specific expressions of the macroscopic equivalent stiffness of a foam-filled corrugated core have been obtained by Han et al. [1] obtained using the method of energy-based homogenization. The assumptions adopted during the homogenization, such as small deformation and linear elasticity, are suitable for the present analysis. Upon removing the relevant terms relevant to foam insertion, the equivalent stiffness of an empty corrugated core can be expressed as:

$$\begin{aligned} C_{11}^H &= \frac{E_1 t_c \cos^3\theta}{(1-\nu_{12}\nu_{21})c} + \frac{E_1}{1-\nu_{12}\nu_{21}}\left(\frac{t_c \sin\theta}{c}\right)^3 \sin\theta\cos\theta \\ C_{22}^H &= \frac{2E_2 t_c \sin\theta}{(1-\nu_{12}\nu_{21})c\sin 2\theta} \\ C_{12}^H &= \frac{\nu_{12}E_2 t_c \cos\theta}{(1-\nu_{12}\nu_{21})c} \\ C_{44}^H &= \frac{E_1}{1-\nu_{13}\nu_{31}}\left[\frac{t_c sin^2\theta\cos\theta}{(1-\nu_{12}\nu_{21})c} + \left(\frac{t_c \sin\theta}{c}\right)^3\frac{(cos^2\theta - sin^2\theta)^2}{4\sin\theta\cos\theta}\right] \\ C_{55}^H &= G_{23}^c\frac{t_c\sin^2\theta}{c\cos\theta} \\ C_{66}^H &= G_{13}^c\frac{t_c\sin^2\theta}{c\cos\theta} \end{aligned} \tag{11}$$

2.4. Energy formulation

The strain energy of the corrugated sandwich plate can be expressed as:

$$\begin{aligned} U &= \frac{1}{2}\sum_{t,c,b}\int_V(\sigma_x\varepsilon_x + \sigma_y\varepsilon_y + \tau_{xy}\gamma_{xy} + \tau_{yz}\gamma_{yz} + \tau_{xz}\gamma_{xz})dV \\ &= \frac{1}{2}\sum_{t,c,b}\int_A\int_z(\{\varepsilon\}^{fT}[\mathbf{C}]^{f}\{\varepsilon\}^{f} + \{\varepsilon\}^{cT}[\mathbf{C}]^{H}\{\varepsilon\}^{c})dzdA \end{aligned} \tag{12}$$

By adopting the assumption of von Karman large deformation and neglecting the membrane deformation, the potential energy contains contributions from both the body force and the terminal load, given by:

$$V = V_P + V_G V_P = -\int_A P\left(\frac{1}{2}\left(\frac{\partial w}{\partial y}\right)^2\right)dA V_G$$
$$= -(\frac{\rho_c g c}{2} + \rho_f g\frac{h-c}{2})\int_A (L-y)\left(\frac{\partial w}{\partial y}\right)^2 dA \tag{13}$$

where ρ_c is the equivalent density of the corrugated core and ρ_f is the material density of the face sheets. The equivalent density ρ_c is given by:

$$\rho_c = \frac{M_{core}}{V_{core}} = \frac{\rho_{cm} t_c \frac{2c}{\sin\theta}}{c\cdot\frac{2c}{\tan\theta}} = \frac{\rho_{cm} t_c}{c\cos\theta} \tag{14}$$

where ρ_{cm} is the material density of the corrugated plate, M_{core} is the mass of a unit cell of the corrugated core and V_{core} represents the corresponding equivalent volume.

3. Solution method and boundary conditions

3.1. Solution method

For generality and convenience, the following non-dimensional terms are introduced:

$$\bar{x} = \frac{x}{L};\quad \bar{y} = \frac{y}{L};\quad \bar{w} = \frac{w}{L};\quad d\bar{A} = d\bar{x}d\bar{y};\quad \bar{P} = \frac{PL^2}{D_{eq}};$$
$$\bar{q} = \frac{\rho_f g t_{eq} L^3}{D_{eq}} \tag{15}$$

in which t_{eq} represents the equivalent thickness of a homogeneous plate having the same mass as the corrugated sandwich and the same material as the face sheets, and D_{eq} represents the equivalent stiffness of the corrugated sandwich plate in the y direction (Fig. 1), given specifically by:

$$t_{eq} = \bar{\rho}_c c + (h-c);\quad \bar{\rho}_c = \frac{\rho_c}{\rho_f};\quad D_{eq} = \int_{-c/2}^{c/2} z^2 C_{22}^H dz + 2\int_{c/2}^{f/2} z^2 C_{22}^f dz \tag{16}$$

Here, $\bar{\rho}_c$ represents the relative density of the corrugated core layer, which is defined in the present study as the ratio of ρ_c to ρ_f.

The p-Ritz method [17] is used to solve the problem of Fig. 1, using the following p-Ritz functions:

$$w(\bar{x},\bar{y}) = \sum_{q=0}^{p}\sum_{i=0}^{q} w_m \psi_m^w(\bar{x},\bar{y}) = \sum_{q=0}^{p}\sum_{i=0}^{q} w_m \phi_b^w(\bar{x},\bar{y})\bar{x}^i\bar{y}^{q-i}$$
$$\alpha_c(\bar{x},\bar{y}) = \sum_{q=0}^{p}\sum_{i=0}^{q} \alpha_m^c \psi_m^{xc}(\bar{x},\bar{y}) = \sum_{q=0}^{p}\sum_{i=0}^{q} \alpha_m^c \phi_b^{xc}(\bar{x},\bar{y})\bar{x}^i\bar{y}^{q-i}$$
$$\beta_c(\bar{x},\bar{y}) = \sum_{q=0}^{p}\sum_{i=0}^{q} \beta_m^c \psi_m^{yc}(\bar{x},\bar{y}) = \sum_{q=0}^{p}\sum_{i=0}^{q} \beta_m^c \phi_b^{yc}(\bar{x},\bar{y})\bar{x}^i\bar{y}^{q-i}$$
$$\alpha_f(\bar{x},\bar{y}) = \sum_{q=0}^{p}\sum_{i=0}^{q} \alpha_m^f \psi_m^{xf}(\bar{x},\bar{y}) = \sum_{q=0}^{p}\sum_{i=0}^{q} \alpha_m^f \phi_b^{xf}(\bar{x},\bar{y})\bar{x}^i\bar{y}^{q-i}$$
$$\beta_f(\bar{x},\bar{y}) = \sum_{q=0}^{p}\sum_{i=0}^{q} \beta_m^f \psi_m^{yf}(\bar{x},\bar{y}) = \sum_{q=0}^{p}\sum_{i=0}^{q} \beta_m^f \phi_b^{yf}(\bar{x},\bar{y})\bar{x}^i\bar{y}^{q-i} \tag{17}$$

where p is the degree of the complete polynomial space, w_i, α_i^c, β_i^c, α_i^f, β_i^f are the unknown coefficients to be varied with the subscript m given by:

$$m = (q+1)(q+2)/2 - i \tag{18}$$

and ϕ_b^w, ϕ_b^{xc}, ϕ_b^{yc}, ϕ_b^{xf}, ϕ_b^{yf} are the basic functions that are set to satisfy geometric boundary conditions [17].

Upon substituting (17) into (4) and (5), the strains can be rewritten as:

$$\{\varepsilon\}^{f,c} = [\mathbf{B}]^{f,c}\{\boldsymbol{\Delta}\} \tag{19}$$

where

$$[\mathbf{B}]^f = \begin{bmatrix} \pm\frac{c}{2}\frac{\partial\psi_b^{xc}}{L\partial\bar{x}} & -(z\pm\frac{c}{2})\frac{\partial\psi_b^{xf}}{L\partial\bar{x}} & 0 & 0 & 0 \\ 0 & 0 & \pm\frac{c}{2}\frac{\partial\psi_b^{yc}}{L\partial\bar{y}} & -(z\pm\frac{c}{2})\frac{\partial\psi_b^{yf}}{L\partial\bar{y}} & 0 \\ \pm\frac{c}{2}\frac{\partial\psi_b^{xc}}{L\partial\bar{y}} & -(z\pm\frac{c}{2})\frac{\partial\psi_b^{xf}}{L\partial\bar{y}} & \pm\frac{c}{2}\frac{\partial\psi_b^{yc}}{L\partial\bar{x}} & -(z\pm\frac{c}{2})\frac{\partial\psi_b^{yf}}{L\partial\bar{x}} & 0 \\ 0 & 0 & 0 & -\psi_b^{yf} & \frac{\partial\psi_b^{w}}{\partial\bar{y}} \\ 0 & -\psi_b^{xf} & 0 & 0 & \frac{\partial\psi_b^{w}}{\partial\bar{x}} \end{bmatrix} \tag{20}$$

$$[\mathbf{B}]^c = \begin{bmatrix} -z\frac{\partial\psi_b^{xc}}{L\partial\bar{x}} & 0 & 0 & 0 & 0 \\ 0 & 0 & -z\frac{\partial\psi_b^{yc}}{L\partial\bar{y}} & 0 & 0 \\ -z\frac{\partial\psi_b^{xc}}{L\partial\bar{y}} & 0 & -z\frac{\partial\psi_b^{yc}}{L\partial\bar{x}} & 0 & 0 \\ 0 & 0 & -\psi_b^{yc} & 0 & \frac{\partial\psi_b^{w}}{\partial\bar{y}} \\ -\psi_b^{xc} & 0 & 0 & 0 & \frac{\partial\psi_b^{w}}{\partial\bar{x}} \end{bmatrix} \tag{21}$$

$$\{\boldsymbol{\Delta}\} = [\alpha_m^c \quad \alpha_m^f \quad \beta_m^c \quad \beta_m^f \quad w_m]^T \tag{22}$$

Accordingly, the strain energy of the corrugated sandwich plate becomes:

$$U = \frac{1}{2}\sum_{t,c,b}\int_{\bar{A}}\int_z (\{\boldsymbol{\Delta}\}^T[\mathbf{B}]^{fT}[\mathbf{C}]^f[\mathbf{B}]^f\{\boldsymbol{\Delta}\}$$
$$+ \{\boldsymbol{\Delta}\}^T[\mathbf{B}]^{cT}[\mathbf{C}]^H[\mathbf{B}]^c\{\boldsymbol{\Delta}\})dzd\bar{A} \tag{23}$$

for which the stiffness matrix of the sandwich can be written as:

$$[\mathbf{K}] = \frac{\partial U}{\partial\{\boldsymbol{\Delta}\}} = \sum_{t,c,b}\int_{\bar{A}}\int_z ([\mathbf{B}]^{fT}[\mathbf{C}]^f[\mathbf{B}]^f + [\mathbf{B}]^{cT}[\mathbf{C}]^H[\mathbf{B}]^c)dzd\bar{A} \tag{24}$$

with:

$$\begin{bmatrix} \mathbf{K}^{\alpha c\alpha c} & \mathbf{K}^{\alpha c\alpha f} & \mathbf{K}^{\alpha c\beta c} & \mathbf{K}^{\alpha c\beta f} & \mathbf{K}^{\alpha cw} \\ & \mathbf{K}^{\alpha f\alpha f} & \mathbf{K}^{\alpha f\beta c} & \mathbf{K}^{\alpha f\beta f} & \mathbf{K}^{\alpha fw} \\ & & \mathbf{K}^{\beta c\beta c} & \mathbf{K}^{\beta c\beta f} & \mathbf{K}^{\beta cw} \\ & \text{Sym} & & \mathbf{K}^{\beta f\beta f} & \mathbf{K}^{\beta fw} \\ & & & & \mathbf{K}^{ww} \end{bmatrix} \tag{25}$$

Explicit expressions of the elements in [**K**] are presented in Appendix A.

Upon substituting (17) into (13), the two contributions of the potential energy can be rewritten as:

$$V_p = -\frac{1}{2}\int_{\bar{A}}\{\boldsymbol{\Delta}\}^T[\mathbf{B}']^T\bar{P}[\mathbf{B}']\{\boldsymbol{\Delta}\}d\bar{A}$$
$$V_G = -\frac{1}{2}\int_{\bar{A}}(1-y)^2\{\boldsymbol{\Delta}\}^T[\mathbf{B}']^T\bar{q}[\mathbf{B}']\{\boldsymbol{\Delta}\}d\bar{A} \tag{26}$$

where

$$[\mathbf{B}'] = \begin{bmatrix} 0 & 0 & 0 & 0 & 0 \\ 0 & 0 & 0 & 0 & 0 \\ 0 & 0 & 0 & 0 & 0 \\ 0 & 0 & 0 & 0 & 0 \\ 0 & 0 & 0 & 0 & \frac{\partial\psi_b^w}{\partial\bar{y}} \end{bmatrix} \tag{27}$$

Finally, the geometric stiffness matrices due to terminal load and body force can be expressed separately by:

$$[\mathbf{K}_P] = -\frac{1}{2}\int_{\bar{A}}[\mathbf{B}']^T\bar{P}[\mathbf{B}']d\bar{A}$$
$$[\mathbf{K}_G] = -\frac{1}{2}\int_{\bar{A}}(1-y)^2[\mathbf{B}']^T\bar{q}[\mathbf{B}']d\bar{A} \tag{28}$$

so that the equilibrium equation for buckling analysis takes the form of:

$$([\mathbf{K}] + [\mathbf{K}_P] + [\mathbf{K}_G])\{\boldsymbol{\Delta}\} = \{\mathbf{0}\} \tag{29}$$

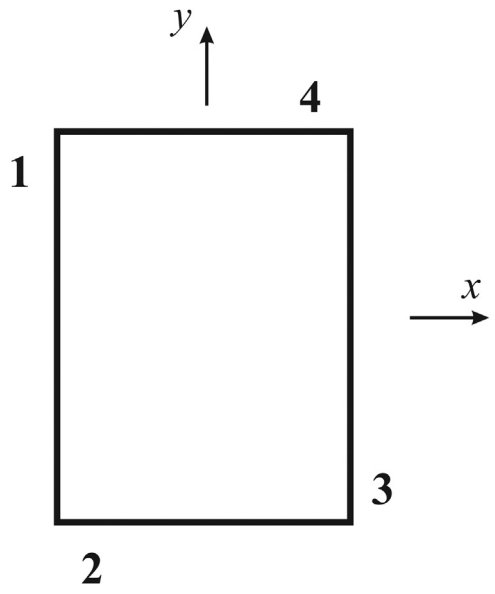

Fig. 3. Order of plate edges for boundary conditions specified in Table 1.

When $\{\mathbf{\Delta}\}$ has non-zero solutions, the determinant of its coefficient matrix should be zero, i.e., $|[\mathbf{K}] + [\mathbf{K}_P] + [\mathbf{K}_G]| = 0$. Note that $[\mathbf{K}_P]$ and $[\mathbf{K}_G]$ contain the two buckling load parameters $\overline{P}$ and $\overline{q}$ to be solved. In the present study, when a specific value is prescribed to $\overline{P}$ or $\overline{q}$, the corresponding critical buckling parameter $\overline{q}$ or $\overline{P}$ is obtained via *MATHEMATICA*.

3.2. Boundary conditions

Theoretically, the p-Ritz method can be used to solve any type of boundary conditions. However, when cost and effectiveness are considered, four different boundary condition types for the four edges of the plate displayed in Fig. 3 are discussed. For example, as listed in Table 1, the boundary condition FCSF means that the 1st edge is free, the 2nd edge is clamped, the 3rd edge is simply-supported, and the 4th edge is Free. For each type of boundary condition, the basic functions are presented in Table 1, which satisfy the geometric boundary conditions as the p-Ritz method requires [17].

4. Buckling results and discussion

4.1. Validation

Since there exists no study on the gravity-induced buckling of corrugated sandwich plate, two approaches are taken to compare and verify the critical buckling parameters calculated using the present theoretical method: (1) the corrugated sandwich plate is degenerated to a homogeneous plate so that the predicted buckling parameters can be compared with existing solutions [5,6]; (2) the critical buckling parameters of the corrugated sandwich plate are calculated numerically using the method of finite elements (FE) and compared with those predicted theoretically.

Table 1
Basic functions under different boundary conditions.

Boundary Conditions	ϕ_b^{xc}/ϕ_b^{xf}	ϕ_b^{yc}/ϕ_b^{yf}	ϕ_b^{w}
FCFF[a](1234[b])	$(\bar{x}+a)^0(\bar{y}+1)^1$	$(\bar{x}+a)^0(\bar{y}+1)^1$	$(\bar{x}+a)^0(\bar{y}+1)^1$
	$(\bar{x}-a)^0(\bar{y}-1)^0$	$(\bar{x}-a)^0(\bar{y}-1)^0$	$(\bar{x}-a)^0(\bar{y}-1)^0$
FSSF(1234)	$(\bar{x}+a)^0(\bar{y}+1)^1$	$(\bar{x}+a)^0(\bar{y}+1)^0$	$(\bar{x}+a)^0(\bar{y}+1)^1$
	$(\bar{x}-a)^0(\bar{y}-1)^0$	$(\bar{x}-a)^1(\bar{y}-1)^0$	$(\bar{x}-a)^1(\bar{y}-1)^0$
FCSF(1234)	$(\bar{x}+a)^0(\bar{y}+1)^1$	$(\bar{x}+a)^0(\bar{y}+1)^1$	$(\bar{x}+a)^0(\bar{y}+1)^1$
	$(\bar{x}-a)^0(\bar{y}-1)^0$	$(\bar{x}-a)^1(\bar{y}-1)^0$	$(\bar{x}-a)^1(\bar{y}-1)^0$
FSSS(1234)	$(\bar{x}+a)^0(\bar{y}+1)^1$	$(\bar{x}+a)^0(\bar{y}+1)^0$	$(\bar{x}+a)^0(\bar{y}+1)^1$
	$(\bar{x}-a)^0(\bar{y}-1)^1$	$(\bar{x}-a)^1(\bar{y}-1)^0$	$(\bar{x}-a)^1(\bar{y}-1)^1$

[a] F: free; C: clamped; S: simply-supported.
[b] Order of plate edges are specified in Fig. 3.

Table 2
Comparison of $\overline{q}$ when $\overline{P} = 0$: homogeneous plate ($a = 0.5$).

Case	FCFF	SSSF	SCSF	CSCF	SSSS
3D FE ($L/h=40$)	7.257	195.646	280.818	325.570	195.858
3D FE ($L/h=100$)	7.357	203.092	287.700	334.454	203.372
Present study ($L/h=40$)	7.456	210.304	299.924	338.818	210.583
Present study ($L/h=100$)	7.473	213.167	305.095	351.423	213.468
Wang et al. [5,6]	7.4752	213.72	306.09	353.95	214.02

*3D FE simulation results are calculated from ABAQUS (Element type: C3D8R); the results from Wang et al. [5,6] did not consider the shear effect, and were independent of L/h.

For the first approach, the stiffness constants of the equivalent corrugated core in Eq. (10) are replaced with those of a homogeneous isotropic plate, i.e., $[\mathbf{C}]^{\mathrm{H}} = [\mathbf{C}]^{\mathrm{f}}$, $E_1^{\mathrm{f}} = E_2^{\mathrm{f}}$, $\nu_{12}^{\mathrm{f}} = \nu_{21}^{\mathrm{f}}$ and $G_{12}^{\mathrm{f}} = G_{23}^{\mathrm{f}} = G_{13}^{\mathrm{f}}$. The critical buckling parameters of a standing vertical homogeneous plate thus obtained are then compared with the 3D FE simulation results and existing solutions, as shown in Table 2 for the case when $\overline{P} = 0$. Six 3D solid elements (C3D8R) are used across the thickness of the plate. Overall, good agreement is achieved. The results of the present study are closer to the 3D FE results than the results of Wang et al. [5,6], as the latter did not consider the shear deformation while the former takes into account the first order shear deformation. As expected, the influence of shear effect gets smaller as the aspect ratio L/h increases, which is consistent with our previous study [18], in which the shear effect is found to decrease with increasing slender ratio L/h.

To determine the relation between $\overline{P}$ and $\overline{q}$ for corrugated sandwich plates, FE calculations using ABAQUS/Standard are implemented for all four types of boundary conditions listed in Table 1. 3D deformable four-node shell elements with reduced integration (S4R) are used to model the corrugated sandwich structure as depicted in Fig. 4. Interactions between the top/bottom face sheet and the corrugated core are assumed to be perfect bonding (Tie). To determine the stability of a corrugated sandwich plate under terminal load and body force, the two step analysis is employed: A general step of static analysis is firstly carried out for calculating the initial stress field under the prescribed "self-weight" with gravity option; subsequently, a linear perturbation step of buckle analysis is applied. For sandwich plates under sole terminal load or body force, only a buckle analysis is needed. Mesh convergence has been guaranteed for each calculation, and the maximal element size used in all FE calculations is 0.008 m. Relevant material parameters of the face sheets and the corrugated plate are: $\rho = 7900\ \mathrm{kg}/m^3$, $\nu = 0.3$ and $E = 210\mathrm{GPa}$. Geometric parameters used in the FE simulations are: $L = 4\mathrm{m}$, $a = 1$, $h = 0.1\mathrm{m}$, $c = 0.09\mathrm{m}$, $t_{\mathrm{c}} = 0.005\mathrm{m}$, $t_{\mathrm{f}} = 0.005\mathrm{m}$ and $\overline{\rho}_{\mathrm{c}} = 0.11$. With global buckling assumed, the first order global buckling results of FE calculations are viewed as the critical buckling parameters and compared with the theoretical predications. The first order global buckling modes calculated from the

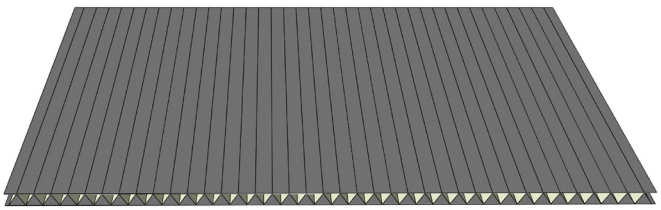

Fig. 4. The model of corrugated sandwich plate adopted in FE calculations (the face sheets and corrugated core are all modelled with 3D deformable shell elements).

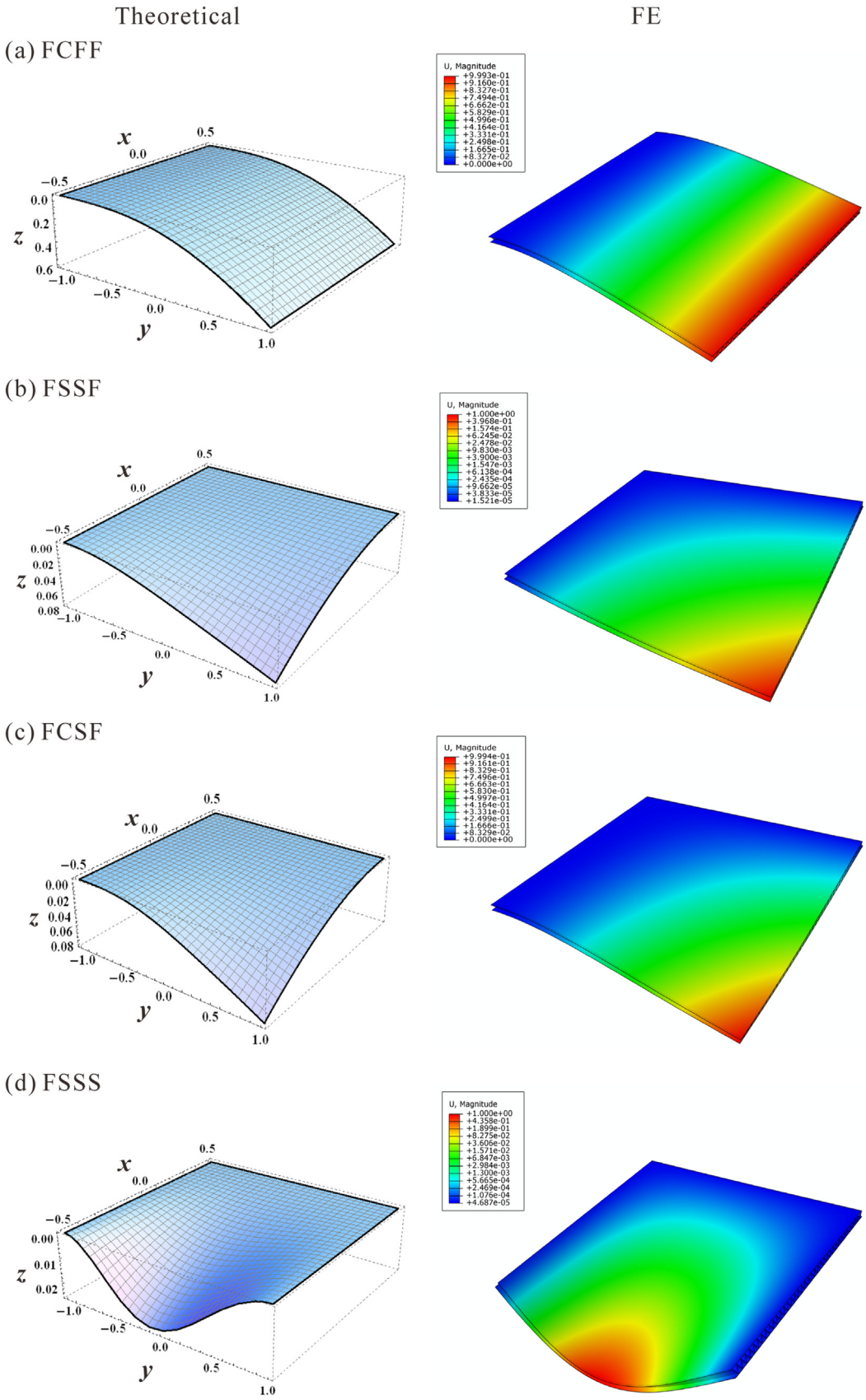

Fig. 5. First order buckling modes under four different types of boundary condition (the sandwich plate is under sole body force): comparison between FE calculations and theoretical predictions.

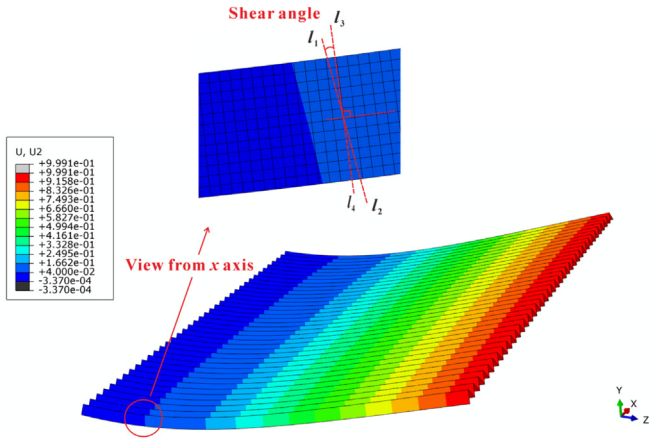

Fig. 6. The way that the FE model considers the shear effect of the core (1st-order buckling mode of corrugated sandwich plate subjected to sole body force with FCFF boundary).

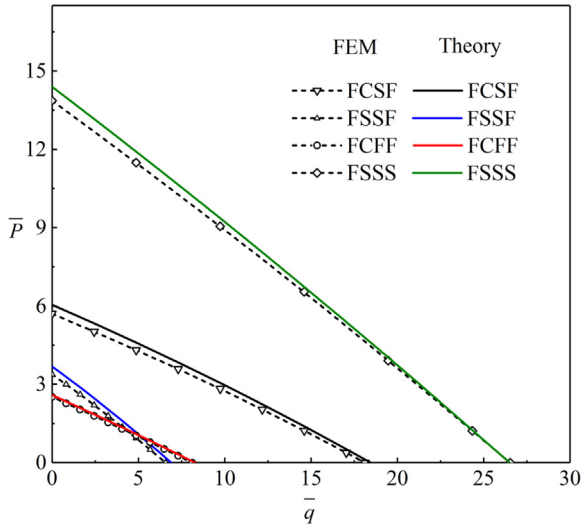

Fig. 7. Comparison between theory and FE simulation: relation between critical buckling parameters of corrugated sandwich plate under body force and terminal load for four different types of boundary condition (Table 1).

FE and the theoretical formulation are compared in Fig. 5, and it is seen that consistent results are obtained. Fig. 6 illustrates the way that the present FE model considers the shear effect of the corrugated core, in which the angle between the line l_1l_2 (equal displacement line) and the line l_3l_4 perpendicular to the mid-plane represents the shear effect. As shown in Fig. 7, for each type of boundary condition considered, the theoretical predictions of critical buckling parameters agree well with the FE results, with a discrepancy less than 3%.

4.2. Shear effect of face sheets

Example 1:. Metal face sheets and metal core

First, the shear effect of metal face sheet is studied when its thickness t_f is increased, as shown in Fig. 8 for a corrugated sandwich plate with FCSF boundary. Unless otherwise stated, solid lines in Fig. 8 (as well as Figs. 9, 11 and 12) refer to results obtained with the shear effect of face sheets taken into account, while the dashed lines denote results obtained without accounting for such effect. The results of not considering the shear effect of face sheets are obtained using the same solution method as mentioned in Section 3. Here, relative to the "Face shear" results, the difference is that the two unknown functions α_f, β_f in Eqs. (1) and (3) are replaced with $\partial w/\partial x$, $\partial w/\partial y$. The results of Fig. 8

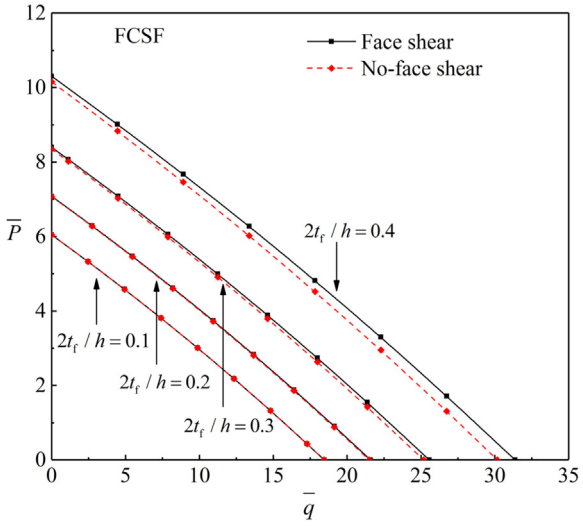

Fig. 8. Shear effect of metal face sheets on critical buckling parameters of corrugated sandwich plate under FCSF constraint for selected face sheet thicknesses ($\theta=\frac{\pi}{3}$, $a=1$, $h/L=1/40$ and $\bar{\rho}_c=0.11$).

demonstrate that shear effect is no longer negligible when the face sheet thickness becomes larger than about 15% of total sandwich thickness (Fig. 1). Note that the range of face sheet thickness considered in plotting Fig. 8 is similar to that used by Kardomateas [13].

To explore further the shear effect, Fig. 9 plots the critical buckling parameters as functions of h/L for different boundary conditions, with $2t_f/h=0.4$. While the shear effect becomes obvious when the ratio of total plate thickness to height increases, it is more apparent under FCFF constraints than under FCSF. This is because the deformation of the sandwich plate becomes smaller when its edges are simply-supported, reducing thus the corresponding shear effect of the face sheets. Further, when the plate is subjected to in-plane uniformly distributed load, like body force, the shear effect is more sensitive to the variation of h/L in comparison with the case when the plate is subjected to terminal load. In sharp contrast, for sandwich plates under FSSF and FSSS constraints, the results of Fig. 9(b) and (d) show that the shear effect is negligibly small within the whole range of geometrical parameters considered.

Example 2:. FGM face sheets and metal core

Consider next the case when the metal face sheets are replaced with FGM face sheets that have metallic inner side and ceramic outer side, as shown in Fig. 10. It is assumed that the material make of the corrugated core plate remains to be metal, thus this change will not influence the connection between the face sheets and the core. For simplicity, the Poisson ratio is assumed to be constant ($\nu=0.3$) for both the FGM face sheets and the core plate, and the Young's modulus of the FGM is assumed to vary according to the following linear expressions [19–21]:

$$E^f(z)=\begin{cases}E_c+(E_m-E_c)\left(\frac{2z+h}{h-c}\right) & z\in\left[-\frac{h}{2},-\frac{c}{2}\right]\\ E_c+(E_m-E_c)\left(\frac{2z-h}{c-h}\right) & z\in\left[\frac{c}{2},\frac{h}{2}\right]\end{cases} \tag{30}$$

where E_c and E_m represent the Young's moduli of ceramic and metal, respectively.

Fig. 11 shows the variation trend of shear effect caused by the change of E_c/E_m under FCSF constraint. The metal is stiffer than ceramic when E_c/E_m is less than 1 and softer than the ceramic when E_c/E_m is greater than 1; when $E_c/E_m=1$, the face sheets are monolithic. From Fig. 11 it is seen that the influence of shear effect on the critical buckling parameters $\bar{P}$ and $\bar{q}$ becomes apparent as E_c/E_m is increased, and both decrease with increasing E_c/E_m.

Example 3:. Composite face sheets and core plate

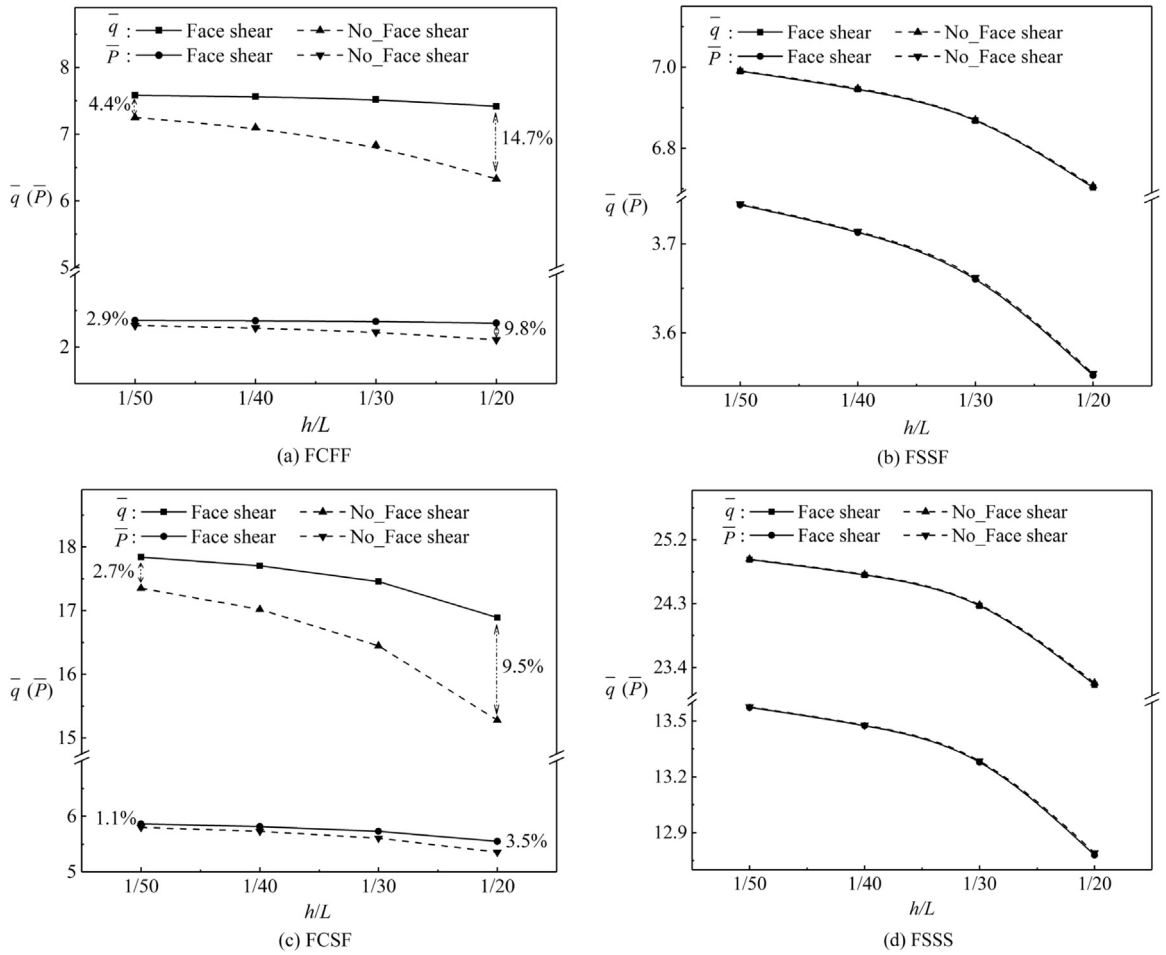

Fig. 9. Shear effect of metal face sheets on critical buckling parameters of corrugated sandwich plate under different boundary conditions ($\theta = \frac{\pi}{3}$, $a = 1$, $h/L = 1/40$, $\bar{\rho}_c = 0.11$ and $2t_f/h = 0.4$).

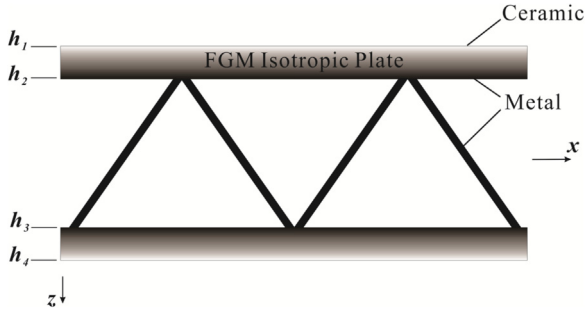

Fig. 10. Corrugated sandwich plate with FGM face sheets.

As a third example, consider an all-composite corrugated sandwich plate. Both its face sheets and core are made of T700/3234, with the following elastic properties [22]: $E_1 = E_3 = 8.7$GPa, $E_2 = 110$GPa, $G_{12} = G_{13} = G_{23} = 4$GPa, $\nu_{13} = 0.3$, $\nu_{21} = \nu_{23} = 0.32$. The main direction of the fiber-reinforced composite material is in line with the y-axis (Fig. 1). For FCSF constraints, Fig. 12 displays the change of shear effect as a result of varying the face sheet thickness. To validate the shear effect of the face sheets, the results of Fig. 12 are obtained by modeling the face sheets with 3D solid elements (C3D8R), which is the different from the FE model depicted in Fig. 4. There are 4 elements in the thickness direction of the face sheets, and it has been established that numerical convergence is guaranteed. As shown in Fig. 12, the difference between the 3D FE results and the present study decreases when the shear effect of face sheets is taken into account. Similar to the

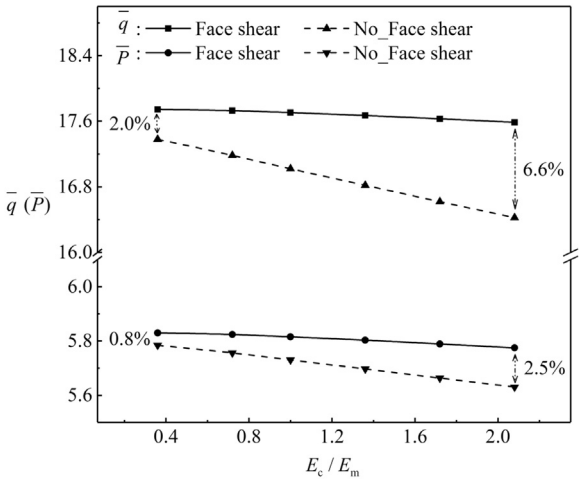

Fig. 11. Shear effect of FGM face sheets on critical buckling parameters of corrugated sandwich plate under FCSF constraint ($\theta = \frac{\pi}{3}$, $a = 1$, $h/L = 1/40$, $\bar{\rho}_c = 0.11$ and $2t_f/h = 0.4$).

previous two examples, the influence of shear effect on critical buckling parameters is significant when the face sheets are relatively thick. For the case of body force, the maximum error can reach 27.34% if shear effect is neglected.

For all the three examples considered thus far, the predicted critical buckling parameters with face sheet shear effect ignored are smaller

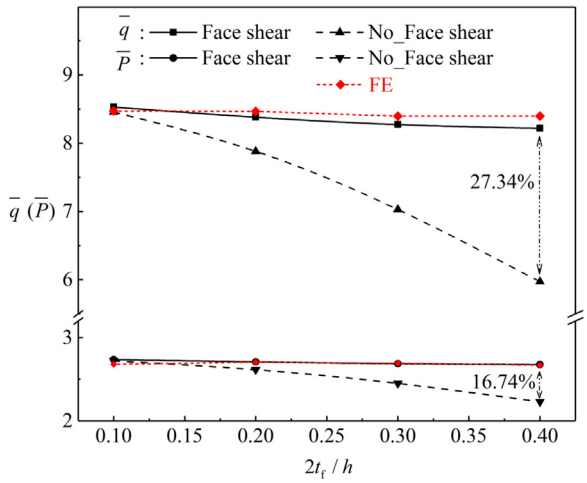

Fig. 12. Critical buckling loads of all-composite (T700/3234) corrugated sandwich plate with FCSF constraint and varying face sheet thickness; FE results are calculated from ABAQUS (Face sheets are modelled with 3D solid elements: C3D8R, and the corrugated core are modelled with 3D shear deformable elements: S4R; $\theta = \frac{\pi}{3}$, $a = 1$, $h/L = 1/40$ and $\bar{\rho}_c = 0.11$).

than those calculated with shear effect duly accounted for. Consequently, in practice, it is conservative to design large-scale sandwich structures without considering the shear deformation of the face sheets.

4.3. Parametric study

The topological parameters of the corrugated sandwich plate that affect its critical buckling parameters ($\bar{P}$ and $\bar{q}$) include: ratio of total thickness to height h/L, ratio of face sheet thickness to total sandwich thickness ratio $2t_f/h$, relative density of corrugated core $\bar{\rho}_c$, inclination angle θ, and plate aspect ratio a ($= W/L$).

With regard the influence of h/L, it can be seen from Fig. 9 that as h/L increases, the critical buckling parameters decrease regardless the type of boundary condition used.

Fig. 13 presents the influence on buckling parameters caused by changing $2t_f/h$ and $\bar{\rho}_c$. It is assumed here that the area density $\bar{M}$ of the structure remains unchanged:

$$\bar{M} = \bar{\rho}_c\left(1 - \frac{2t_f}{h}\right) + \frac{2t_f}{h} \tag{31}$$

so that when $2t_f/h$ decreases, $\bar{\rho}_c$ increases. From Fig. 13, the buckling parameters are seen to increase under FCFF constraint and decrease under FSSF, whereas under both FCSF and FSSS constraints a peak appears on each curve (although the peak under FCSF is rather weak).

With regard to the influence of inclination angle θ, it can be seen from Fig. 14 that $\bar{P}$ and $\bar{q}$ increase monotonically as θ is increased under FCFF and FCSF boundary conditions, and the increase is more rapid under FCSF. Under FSSF and FSSS boundary conditions, however, peaks appear on both the $\bar{P}$ and $\bar{q}$ curves and the peaks do not appear at the same inclination angle. Further, the variation of $\bar{q}$ is more significant than that of $\bar{P}$.

Finally, the variation trends of $\bar{P}$ and $\bar{q}$ brought by varying the aspect ratio a are displayed in Fig. 15. As a is increased, while $\bar{P}$ and $\bar{q}$

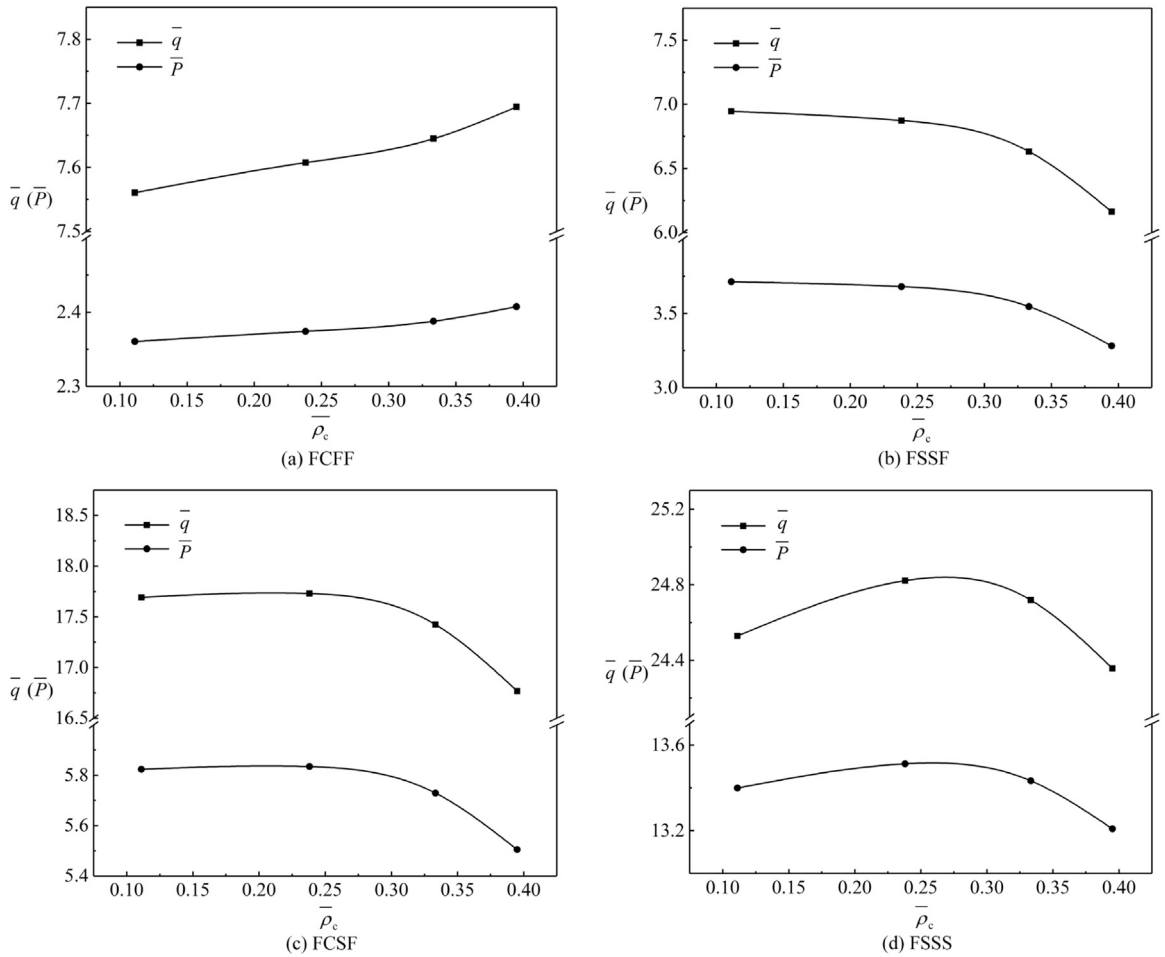

Fig. 13. Critical buckling parameters plotted as functions of relative density $\bar{\rho}_c$ under different boundary conditions, with $\theta = \frac{\pi}{3}$, $a = 1$ and $h/L = 1/40$.

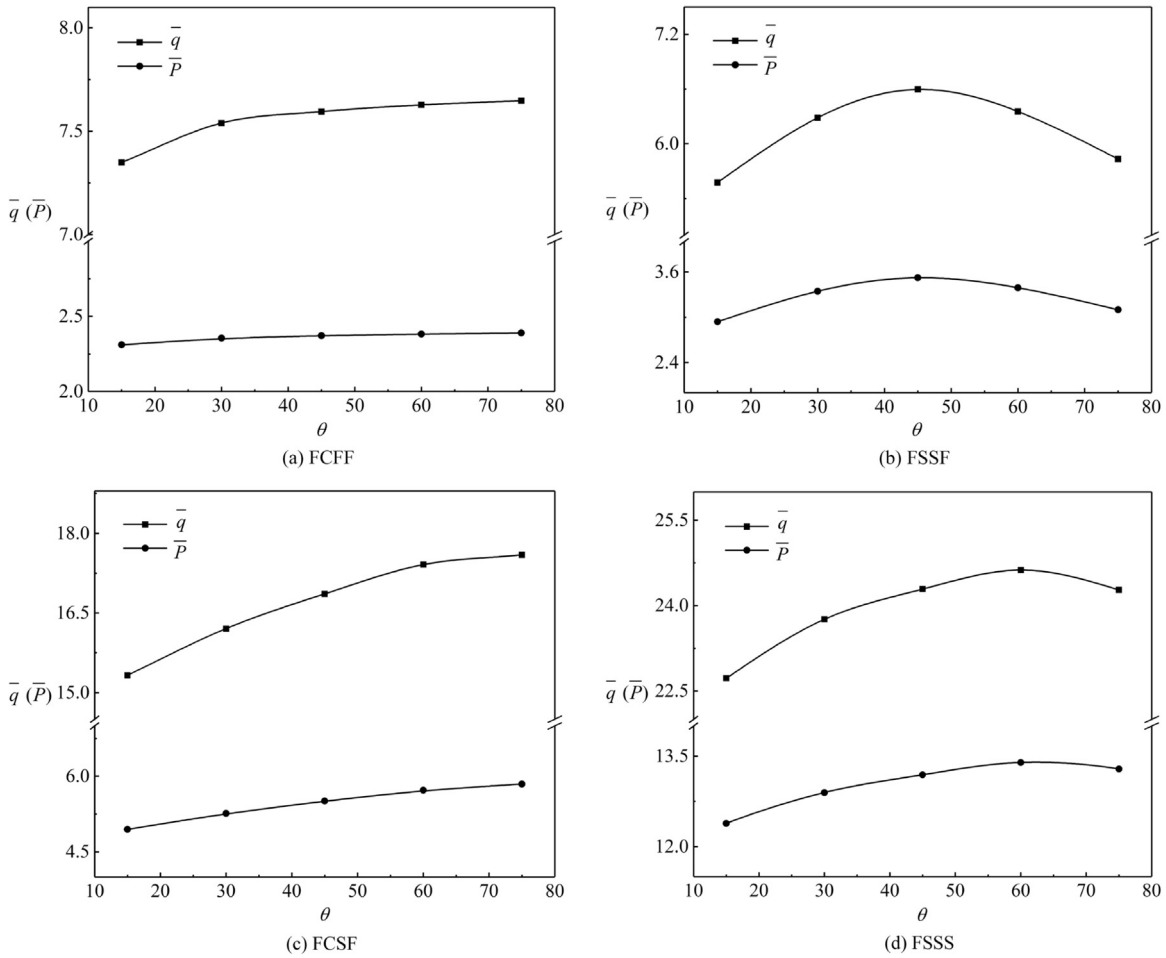

Fig. 14. Critical buckling parameters plotted as functions of inclination angle θ under different boundary conditions, with $a = 1$, $h/L = 1/40$, $\overline{\rho_c} = 0.11$ and $2t_f/h = 0.1$.

increase slightly under FCFF, they decrease under other three boundary conditions. For both $\overline{P}$ and $\overline{q}$, the variation is more rapid when $a < 1$.

5. Conclusions

The global buckling behavior of a standing corrugated sandwich plate subjected to body force and terminal load has been analyzed under four different types of boundary condition. The effect of shear deformation in the face sheets on critical buckling loads is considered using an improved first order zig-zag shear deformation theory. The validity of theoretical predictions is checked against existing solutions as well as full numerical simulation results. The main conclusions are:

(1) The gravity buckling parameter decreases almost linearly with increasing terminal load for all the cases considered in the present study.
(2) The transverse shear effect of face sheets has significant influence on the critical buckling parameters of corrugated sandwich plates with relatively thick face sheets and small aspect ratio of sandwich plate.
(3) The shear effect of face sheets is more obvious when the structure is subjected to in-plane uniformly distributed load (e.g., body force) rather than terminal load.
(4) The critical buckling parameters increase with increasing relative density $\overline{\rho_c}$ under FCFF constraints, but exhibit opposite trend under FSSF. In contrast, under either FCSF or FSSS constraints, the buckling parameters peak when $\overline{\rho_c}$ is approximate 0.25.
(5) The critical buckling parameters increase with increasing inclination angle under FCFF and FCSF. In contrast, these parameters peak when the angle is approximately 45° under FSSF and 60° under FSSS.
(6) The buckling parameters decrease with increasing aspect ratio under FSSF, FCSF and FSSS constraints, while an opposite trend is observed under FCFF.

The present results demonstrate that the shear effect of face sheets can be significantly large and that the body force plays a vital role in the buckling behavior of corrugated sandwich plates, which are useful for the design and analysis of large-scale corrugated sandwich plates in engineering applications.

Acknowledgements

This work was supported by the National Natural Science Foundation of China (11472209 and 11472208), the China Postdoctoral Science Foundation (2016M600782), the Postdoctoral Scientific Research Project of Shaanxi Province (2016BSHYDZZ18), Zhejiang Provincial Natural Science Foundation of China (LGG18A020001), the Fundamental Research Funds for Xian Jiaotong University (xjj2015102), and the Jiangsu Province Key Laboratory of High-end Structural Materials (hsm1305).

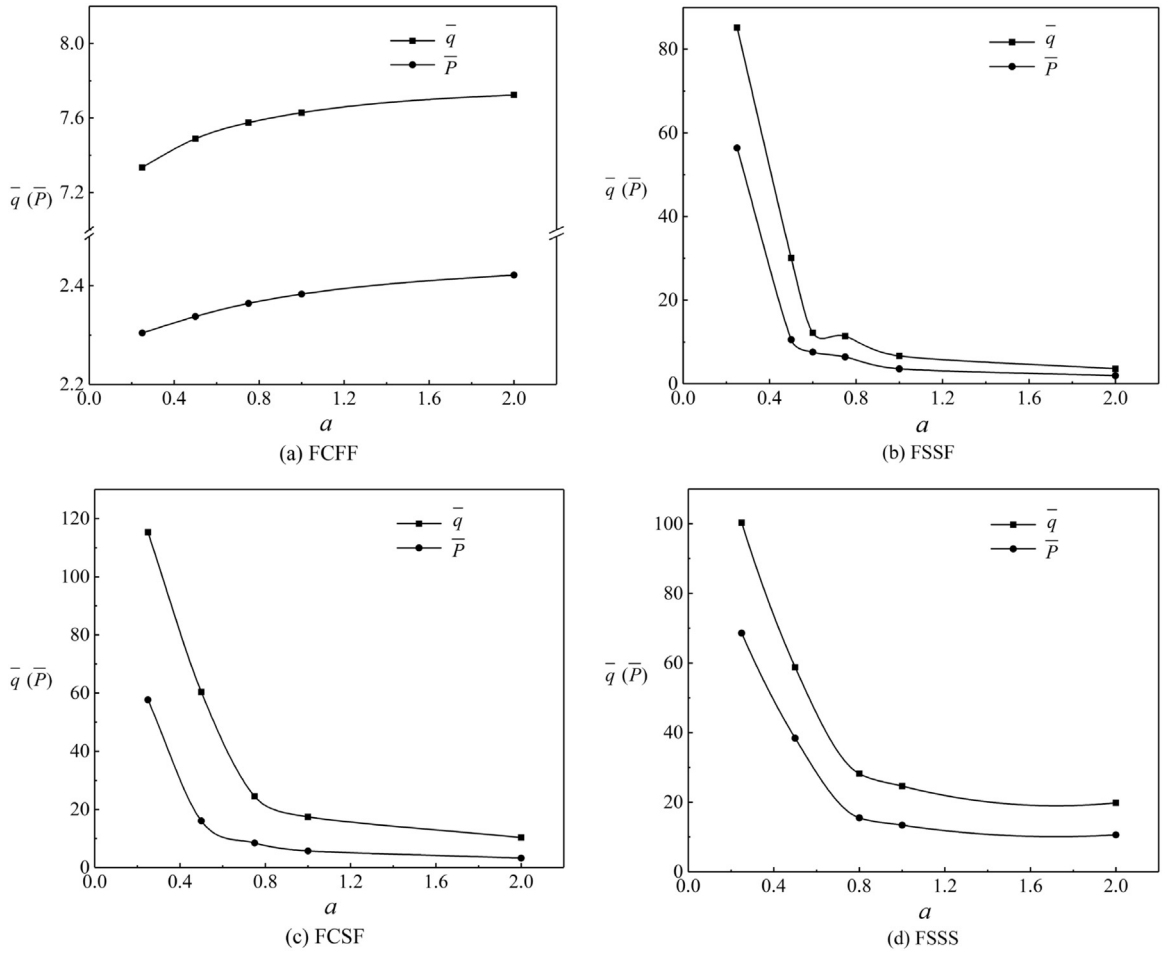

Fig. 15. Critical buckling parameters plotted as functions of plate aspect ratio a under different boundary conditions, with $\theta = \frac{\pi}{3}$, $h/L = 1/40$, $\bar{\rho}_c = 0.11$ and $2t_f/h = 0.1$.

Appendix A . . Elements of stiffness matrix [K] for corrugated sandwich plate

The stiffness matrix **[K]** of Eq. (25) for a corrugated sandwich plate have the following elements:

$$K_{ij}^{\alpha c\alpha c} = \frac{1}{D_{eq}}\left\{\left(\int_{-c/2}^{c/2} z^2 C_{11}^H dz + \int_{c/2}^{h/2} (\frac{c}{2})^2 C_{11}^f dz\right)\int_A \frac{\partial \phi_i^{xc}}{\partial \overline{x}}\frac{\partial \phi_j^{xc}}{\partial \overline{x}} d\overline{A} + \left(\int_{-c/2}^{c/2} z^2 C_{44}^H dz + \int_{c/2}^{h/2} (\frac{c}{2})^2 C_{44}^f dz\right)\int_A \frac{\partial \phi_i^{xc}}{\partial \overline{y}}\frac{\partial \phi_j^{xc}}{\partial \overline{y}} d\overline{A} + L^2 \int_{-c/2}^{c/2} C_{66}^H dz \int_A \phi_i^{xc}\phi_j^{xc} d\overline{A}\right\} \tag{A.1}$$

$$K_{ij}^{\alpha c\alpha f} = -\frac{1}{D_{eq}}\left\{\begin{array}{l}\int_{c/2}^{h/2}\left[(\frac{c}{2})^2 + z{\cdot}c\right] C_{11}^f dz \int_A \frac{\partial \phi_i^{xc}}{\partial \overline{x}}\frac{\partial \phi_j^{xf}}{\partial \overline{x}} d\overline{A} \\ + \int_{c/2}^{h/2}\left[(\frac{c}{2})^2 + z{\cdot}c\right] C_{44}^f dz \int_A \frac{\partial \phi_i^{xc}}{\partial \overline{y}}\frac{\partial \phi_j^{xf}}{\partial \overline{y}} d\overline{A}\end{array}\right\} \tag{A.2}$$

$$K_{ij}^{\alpha c\beta c} = \frac{1}{D_{eq}}\left\{\int_{-c/2}^{c/2} z^2 C_{12}^H dz \int_A \frac{\partial \phi_i^{xc}}{\partial \overline{x}}\frac{\partial \phi_j^{yc}}{\partial \overline{y}} d\overline{A} + \int_{-c/2}^{c/2} z^2 C_{12}^H dz \int_A \frac{\partial \phi_i^{xc}}{\partial \overline{x}}\frac{\partial \phi_j^{xf}}{\partial \overline{y}} d\overline{A} + \int_{c/2}^{h/2} (\frac{c}{2})^2 C_{12}^f dz \int_A \frac{\partial \phi_i^{xc}}{\partial \overline{x}}\frac{\partial \phi_j^{yc}}{\partial \overline{y}} dA + \int_{c/2}^{h/2} (\frac{c}{2})^2 C_{44}^f dz \int_A \frac{\partial \phi_i^{xc}}{\partial \overline{y}}\frac{\partial \phi_j^{yc}}{\partial \overline{x}} d\overline{A}\right\} \tag{A.3}$$

$$K_{ij}^{\alpha c\beta f} = -\frac{1}{D_{eq}}\left\{\begin{array}{l}\int_{c/2}^{h/2}\left[(\frac{c}{2})^2 + z{\cdot}c\right] C_{12}^f dz \int_A \frac{\partial \phi_i^{xc}}{\partial \overline{x}}\frac{\partial \phi_j^{yf}}{\partial \overline{y}} d\overline{A} \\ + \int_{c/2}^{h/2}\left[(\frac{c}{2})^2 + z{\cdot}c\right] C_{44}^f dz \int_A \frac{\partial \phi_i^{xc}}{\partial \overline{y}}\frac{\partial \phi_j^{yf}}{\partial \overline{x}} d\overline{A}\end{array}\right\} \tag{A.4}$$

$$K_{ij}^{\alpha cw} = -\frac{L^2}{D_{eq}} \int_{-c/2}^{c/2} C_{66}^H dz \int_A \phi_i^{xc} \frac{\partial \phi_j^{w}}{\partial \overline{x}} d\overline{A} \tag{A.5}$$

$$K_{ij}^{\alpha f\alpha f}=\frac{1}{D_{\mathrm{eq}}}\left\{\int_{c/2}^{h/2}(z+\frac{c}{2})^2C_{11}^{f}dz\int_{\overline{A}}\frac{\partial\phi_i^{xf}}{\partial\overline{x}}\frac{\partial\phi_j^{xf}}{\partial\overline{x}}d\overline{A}+\int_{c/2}^{h/2}(z+\frac{c}{2})^2C_{44}^{f}dz\int_{\overline{A}}\frac{\partial\phi_i^{xf}}{\partial\overline{y}}\frac{\partial\phi_j^{xf}}{\partial\overline{y}}d\overline{A}+L^2\int_{c/2}^{h/2}C_{66}^{f}dz\int_{\overline{A}}\phi_i^{xf}\phi_j^{xf}d\overline{A}\right\} \tag{A.6}$$

$$K_{ij}^{\alpha f\beta c}=-\frac{1}{D_{\mathrm{eq}}}\left\{\left[\int_{c/2}^{h/2}(\frac{c}{2})^2C_{12}^{f}dz+\int_{c/2}^{h/2}z\cdot\frac{c}{2}C_{12}^{f}dz\right]\int_{\overline{A}}\frac{\partial\phi_i^{xf}}{\partial\overline{x}}\frac{\partial\phi_j^{yc}}{\partial\overline{y}}d\overline{A}+\left[\int_{c/2}^{h/2}(\frac{c}{2})^2C_{44}^{f}dz+\int_{c/2}^{h/2}z\cdot\frac{c}{2}C_{44}^{f}dz\right]\int_{\overline{A}}\frac{\partial\phi_i^{xf}}{\partial\overline{y}}\frac{\partial\phi_j^{yc}}{\partial\overline{x}}d\overline{A}\right\} \tag{A.7}$$

$$K_{ij}^{\alpha f\beta f}=\frac{1}{D_{\mathrm{eq}}}\left\{\begin{array}{l}\int_{c/2}^{h/2}(z+\frac{c}{2})^2C_{12}^{f}dz\int_{A}\frac{\partial\phi_i^{xf}}{\partial\overline{x}}\frac{\partial\phi_j^{yf}}{\partial\overline{y}}d\overline{A}\\+\int_{c/2}^{h/2}(z+\frac{c}{2})^2C_{44}^{f}dz\int_{A}\frac{\partial\phi_i^{xf}}{\partial\overline{y}}\frac{\partial\phi_j^{yf}}{\partial\overline{x}}d\overline{A}\end{array}\right\} \tag{A.8}$$

$$K_{ij}^{\alpha fw}=-\frac{L^2}{D_{\mathrm{eq}}}\int_{c/2}^{h/2}C_{66}^{f}dz\int_{\overline{A}}\phi_i^{xf}\frac{\partial\phi_j^{w}}{\partial\overline{x}}d\overline{A} \tag{A.9}$$

$$K_{ij}^{\beta c\beta c}=\frac{1}{D_{\mathrm{eq}}}\left\{\begin{array}{l}\left[\int_{-c/2}^{c/2}z^2C_{22}^{H}dz+\int_{c/2}^{h/2}(\frac{c}{2})^2C_{22}^{f}dz\right]\int_{\overline{A}}\frac{\partial\phi_i^{yc}}{\partial\overline{y}}\frac{\partial\phi_j^{yc}}{\partial\overline{y}}d\overline{A}+\left[\int_{-c/2}^{c/2}z^2C_{44}^{H}dz+\int_{c/2}^{h/2}(\frac{c}{2})^2C_{44}^{f}dz\right]\int_{\overline{A}}\frac{\partial\phi_i^{yc}}{\partial\overline{x}}\frac{\partial\phi_j^{yc}}{\partial\overline{x}}d\overline{A}\\+L^2\int_{-c/2}^{c/2}C_{55}^{H}dz\int_{\overline{A}}\phi_i^{yc}\phi_j^{yc}d\overline{A}\end{array}\right\} \tag{A.10}$$

$$K_{ij}^{\beta c\beta f}=-\frac{1}{D_{\mathrm{eq}}}\left\{\left[\int_{c/2}^{h/2}(\frac{c}{2})^2C_{22}^{f}dz+\int_{c/2}^{h/2}z\cdot\frac{c}{2}C_{22}^{f}dz\right]\int_{\overline{A}}\frac{\partial\phi_i^{yc}}{\partial\overline{y}}\frac{\partial\phi_j^{yf}}{\partial\overline{y}}d\overline{A}+\left[\int_{c/2}^{h/2}(\frac{c}{2})^2C_{44}^{f}dz+\int_{c/2}^{h/2}z\cdot\frac{c}{2}C_{44}^{f}dz\right]\int_{\overline{A}}\frac{\partial\phi_i^{yc}}{\partial\overline{x}}\frac{\partial\phi_j^{yf}}{\partial\overline{x}}d\overline{A}\right\} \tag{A.11}$$

$$K_{ij}^{\beta cw}=-\frac{L^2}{D_{\mathrm{eq}}}\int_{-c/2}^{c/2}C_{55}^{H}dz\int_{\overline{A}}\phi_i^{yc}\frac{\partial\phi_j^{w}}{\partial\overline{y}}d\overline{A} \tag{A.12}$$

$$K_{ij}^{\beta f\beta f}=\frac{1}{D_{\mathrm{eq}}}\left\{\int_{c/2}^{h/2}(z+\frac{c}{2})^2C_{22}^{f}dz\int_{\overline{A}}\frac{\partial\phi_i^{yf}}{\partial\overline{y}}\frac{\partial\phi_j^{yf}}{\partial\overline{y}}d\overline{A}+\int_{c/2}^{h/2}(z+\frac{c}{2})^2C_{44}^{f}dz\int_{\overline{A}}\frac{\partial\phi_i^{yf}}{\partial\overline{x}}\frac{\partial\phi_j^{yf}}{\partial\overline{x}}d\overline{A}+L^2\int_{c/2}^{h/2}C_{66}^{f}dz\int_{\overline{A}}\phi_i^{yf}\phi_j^{yf}d\overline{A}\right\} \tag{A.13}$$

$$K_{ij}^{\beta fw}=-\frac{L^2}{D_{\mathrm{eq}}}\int_{c/2}^{h/2}C_{55}^{f}dz\int_{\overline{A}}\phi_i^{yf}\frac{\partial\phi_j^{w}}{\partial\overline{y}}d\overline{A} \tag{A.14}$$

$$K_{ij}^{ww}=\frac{1}{D_{\mathrm{eq}}}\left\{\begin{array}{l}\left[\int_{-c/2}^{c/2}C_{55}^{H}dz+\int_{c/2}^{h/2}C_{55}^{f}dz\right]\int_{\overline{A}}\frac{\partial\phi_i^{w}}{\partial\overline{y}}\frac{\partial\phi_j^{w}}{\partial\overline{y}}d\overline{A}\\+\left[\int_{-c/2}^{c/2}C_{66}^{H}dz+\int_{c/2}^{h/2}C_{66}^{f}dz\right]\int_{\overline{A}}\frac{\partial\phi_i^{w}}{\partial\overline{x}}\frac{\partial\phi_j^{w}}{\partial\overline{x}}d\overline{A}\end{array}\right\} \tag{A.15}$$

References

[1] B. Han, Z.J. Zhang, Q.C. Zhang, Q. Zhang, T.J. Lu, B.H. Lu, Free vibration and buckling analysis of foam-filled composite corrugated sandwich plates under thermal loading, Compos. Struct. 172 (2017) 173–189.

[2] B. Han, Z.J. Zhang, Q.C. Zhang, Q. Zhang, T.J. Lu, B.H. Lu, Recent advances in hybrid lattice-cored sandwiches for enhanced multifunctional performance, EML 10 (2017) 58–69.

[3] T.M. Wang, J.M. Sussaman, Elastic stability of a simply supported plate under linearly variable compressive stresses, AIAA J. 5 (1967) 1362–1364.

[4] C.J. Brown, Elastic buckling of plates subjected to distributed tangential loads, Comput. Struct. 41 (1991) 151–1565.

[5] C.M. Wang, Y. Xiang, C.Y. Wang, Buckling of standing vertical plates under body forces, Int. J. Struct. Stab. Dy. 2 (2002) 151–161.

[6] C.Y. Wang, Buckling of a heavy standing plate with top load, Thin-Walled Struct. 48 (2010) 127–133.

[7] M. Bodaghi, A.R. Saidi, Buckling behavior of standing laminated Mindlin plates subjected to body force and vertical loading, Compos. Struct. 93 (2011) 538–547.

[8] G. Fauconneau, R.D. Marangoni, Natural frequencies and elastic stability of a simply-supported rectangular plate under linearly varying compressive loads, Int. J. Solids Struct. 7 (1971) 473–493.

[9] L.H. Yu, C.Y. Wang, Fundamental frequency of a standing heavy plate with vertical simply-supported edges, J. Sound Vib. 321 (2009) 1–7.

[10] L.H. Yu, C.Y. Wang, Vibration of a standing plate with simply supported vertical sides and weakened by a horizontal hinge, Thin-Walled Struct. 49 (2011) 899–901.

[11] E. Carrera E, S. Birschetto S, A survey with numerical assessment of classical and refined theories for the analysis of sandwich plates, Appl. Mech. Rev. 62 (2009) 010803–010817.

[12] R. Zhao, K. Yu, G.M. Hulbert, Y. Wu, X. Li, Piecewise shear deformation theory and finite element formulation for vibration analysis of laminated composite and sandwich plates in thermal environments, Compos. Struct. 160 (2017) 1060–1083.

[13] G.A. Kardomateas GA, An elasticity solution for the global buckling of sandwich beams/wide panels with orthotropic phases, J. Appl. Mech. 77 (2007) 02015.

[14] K. Swaminathan, D.M. Sangeetha, Thermal analysis of FGM plates - a critical review of various modeling techniques and solution methods, Compos. Struct. 160 (2017) 43–60.

[15] M. Krzysztof, M.B. Ewa, W. Leszek, Elastic bending and buckling of a steel composite beam with corrugated main core and sandwich faces - theoretical study, Appl. Math. Model. 40 (2016) 1276–1286.

[16] J. Lou, B. Wang, L. Ma, L. Wu, Free vibration analysis of lattice sandwich beams under several typical boundary conditions, Acta Mech. Sin. 26 (2013) 458–467.

[17] C.M. Wang, T.M. Aung, Plastic buckling analysis of thick plates using p-Ritz method [J], Int. J. Solids Struct. 44 (2007) 6239–6255.

[18] B. Han, F. Li, Q. Zhang, C. Chen, T.J. Lu, Stability and initial post-buckling of a standing sandwich beam under terminal force and self-weight, Arch. Appl. Mech. 86 (2016) 1063–1082.

[19] P.V. Thuc, H.T. Thai, T.K. Nguyen, A quasi-3D theory for vibration and buckling of functionally graded sandwich beams, Compos. Struct. 119 (2015) 1–12.

[20] Y.W. Kim, Effect of partial elastic foundation on free vibration of fluid-filled functionally graded cylindrical shells, Acta Mech. Sin.-PRC 31 (2015) 920–930.

[21] T.F. Xu, Y.F. Xing, Closed-form solutions for free vibration of rectangular FGM thin plates resting on elastic foundation, Acta Mech. Sin.-RPC 32 (2016) 1088–1103.

[22] M. Li, L.Z. Wu, L. Ma, Structural response of all-composite pyramidal truss core sandwich columns in end compression, Compos. Struct. 93 (2011) 1964–1972.